Biogeosciences Discuss., 10, 1–30, 2013
www.biogeosciences-discuss.net/10/1/2013/
doi:10.5194/bgd-10-1-2013
© Author(s) 2013. CC Attribution 3.0 License.

Biogeosciences
Discussions
Open Access

This discussion paper is/has been under review for the journal Biogeosciences (BG).
Please refer to the corresponding final paper in BG if available.

On the consistency in variations of chlorophyll *a* concentration in the South China Sea as revealed by three remote sensing datasets

S. L. Shang[1,2], Q. Dong[2], C. M. Hu[3], G. Lin[1], Y. H. Li[1], and S. P. Shang[1,2]

[1]Key Laboratory of Underwater Acoustic Communication and Marine Information Technology, Xiamen University, Ministry of Education of China, Xiamen 361005, China
[2]Research and Development Center for Ocean Observation Technologies, Xiamen University, Xiamen 361005, China
[3]College of Marine Science, University of South Florida, 140 Seventh Ave. S., St. Petersburg, FL 33701, USA

Received: 10. April 2013 – Accepted: 15 April 2013 – Published:

Correspondence to: S. L. Shang (slshang@xmu.edu.cn)

Published by Copernicus Publications on behalf of the European Geosciences Union.

CC BY

Abstract

Chlorophyll *a* (Chl) concentrations derived from satellite measurements have been used in oceanographic research, for example to interpret eco-responses to environmental changes on global and regional scales. However, it is unclear how existing Chl products compare with each other in terms of accuracy and consistency in revealing temporal and spatial patterns, especially in the optically complex marginal seas. In this study, we examined three MODIS Chl data products that have been made available to the community by the US NASA using community-accepted algorithms and default parameterization. These included the products derived from the OC3M, GSM and GIOP algorithms. We compared their temporal variations and spatial distributions in the South China Sea. We found that the three products appeared to capture general features such as unique winter peak at the Southeast Asian Time-series Study station (SEATS, 18° N, 116° E), strong upwelling induced bloom off the Vietnam and the Pearl River plume associated bloom in summer, their absolute magnitude, however, may be questionable. Further error statistics using field measured Chl as the truth demonstrated that the three MODIS Chl products may contain high degree of uncertainties in the study region. Root mean square error (RMSE) of the products from OC3M and GSM (on a log scale) was about 0.4 and average percentage error (ε) was $\sim 150\,\%$ (Chl between 0.03–7.67 mg m^{-3}, $n = 63$). In contrast, the GIOP with default parameterization led to higher errors ($\varepsilon = 349\,\%$). This study thus advocates more careful interpretation of Chl spatio-temporal variations when using standard Chl products, and also points to the need of local tuning of algorithm parameterization for the study region.

1 Introduction

Chlorophyll *a* is the primary phytoplankton pigment for photosynthesis, whose concentration (hereafter abbreviated as Chl, mg m^{-3}) has been commonly used as a phytoplankton biomass index by oceanographers. Over the past three decades, an

BGD

10, 1–30, 2013

CC BY

unprecedented view of the spatio-temporal pattern of Chl in the global ocean has been enabled by ocean color satellites such as CZCS, SeaWiFS and MODIS (McClain, 2009). Based on these observations, a better understanding of the ecosystem health and carbon cycling associated with environmental changes at both global and regional scales has been achieved (e.g., Behrenfeld and Boss, 2006). Although the retrieval of Chl from satellite measurements is often problematic in optically complex coastal waters (e.g., Carder et al., 1989), and the use of optical indices for phytoplankton pigmentation has become increasingly accepted (e.g., Cullen, 1982; Marra et al., 2007; Lee et al., 2011; Hirawake et al., 2011; Shang et al., 2011), Chl remains a basic, routinely sampled, and widely accepted oceanographic parameter for oceanographers. Currently, there are three standard (operational) MODIS Chl data products provided by the US NASA Ocean Biology Processing Group (OBPG, http://oceancolor.gsfc.nasa.gov), which are derived from the same MODIS remote sensing reflectance (R_{rs}, sr^{-1}) after atmosphere correction of MODIS measurements over the ocean. The algorithms used to derive these products are the OC3M blue/green band ratio algorithm (O'Reilly et al., 2000), a semi-analytical inversion algorithm (GSM, Maritorena et al., 2002), and a generalized IOP algorithm (GIOP, Franz and Werdell, 2010). It has been well recognized that each algorithm has its own strengths and weaknesses (e.g., O'Reilly et al., 1998; Werdell, 2009). However, while an increasing number of users from the oceanographic community are using the various Chl products to interpret biogeochemical processes or temporal changes, the consistency between these Chl products is generally unknown, especially for marginal seas. Can certain spatio-temporal patterns be revealed by one Chl product but masked by another?

In this study, using an extensive dataset collected from a marginal sea we attempted to address this question. We chose the South China Sea (SCS) as the study region, not only because of the extensive effort in the past decade to collect field data but also because of its regional and global importance (Hong et al., 2011; Palacz et al., 2011; Xiu and Chai, 2011; Lin et al., 2010). Indeed, the SCS is the second largest marginal sea in the world.

BGD
10, 1–30, 2013

CC BY

The study focus is on three standard MODIS Chl products, i.e. Chl products derived from OC3M, GSM, and GIOP (hereafter abbreviated as C_OC3M, C_GSM, and C_GIOP). Our goal is to demonstrate the consistency or discrepancy among the biogeochemical features in the SCS derived from these three easily accessible Chl products, and to diagnose potential reasons of product inconsistency or high uncertainty. Specifically, the analysis was through (1) comparison of Chl spatio-temporal variations at SEATS (a time series station in the SCS), three typical upwelling zones, and the Pearl River estuary; (2) evaluation of MODIS-derived R_{rs} and MODIS Chl products using field measured R_{rs} and Chl as the truth.

2 Data and methods

MODIS monthly mean and monthly climatology data products of Chl (C_OC3M, C_GSM, and C_GIOP) and sea surface temperature (SST) during 2002–2012 were obtained from the US NASA OBPG (http://oceancolor.gsfc.nasa.gov/) using the most recent updates in calibration and algorithms (reprocessing R2012.0). These data products were derived from the daily data after global binning to a spatial resolution of approximately $4 \times 4\,km^2$ at the equator. Data were extracted from the SCS (105–121° E and 10–25° N) for further analysis of spatial and temporal patterns.

MODIS data products were also validated against concurrent in situ measurements. In this analysis, both MODIS R_{rs} and in situ R_{rs} were used to test the algorithm performance. Daily MODIS data at original resolution (approximately 1 km at the equator) were obtained from the same NASA group, and in situ R_{rs} and Chl data were collected from targeted and opportunistic cruise surveys between 2003 and 2011 (Fig. 1), where the measurement details can be found in (Shang et al., 2011). Briefly, R_{rs} data were collected with an above-water GER 1500 spectroradiometer (Spectra Vista Corporation, USA). Water samples were collected from a CTD rosette, from which Chl was measured flurometrically (Lalli and Parsons, 1993).

BGD
10, 1–30, 2013

cc BY

For comparison between MODIS and in situ measurements, the temporal difference was allowed to be $< \pm 48$ h to allow for sufficient number of matchups for statistical analysis. MODIS data associated with the following quality control flags were discarded: atmospheric correction warning, sun glint, high radiance, large viewing angle, large sun angle, clouds, stray light, low water-leaving radiance, Chl algorithm failure, questionable navigation, and dark pixel. In total, we compiled 63 pairs of MODIS R_{rs} and in situ Chl data, 49 pairs of MODIS R_{rs} and in situ R_{rs} data, and 192 pairs of in situ R_{rs} and in situ Chl data. These data covered a wide range of environmental settings, with Chl ranging from 0.03 mg m^{-3} in the oligotrophic South China Sea to 51.15 mg m^{-3} in estuarine waters.

The three algorithms were implemented in IDL to estimate Chl from the spectral R_{rs}. The OC3M parameterization was obtained from the NASA OBPG. The GSM algorithm was downloaded from the International Ocean Color Coordination Group (IOCCG, http://www.ioccg.org/groups/software.html), with necessary modifications to adjust for the wavelength shift from SeaWiFS to MODIS (S. Maritorena, personal communication, 2012). The GIOP algorithm with its default parameterization was taken from Brewin et al. (2012).

To assess the similarity or difference between measured and algorithm-derived parameters, four statistical indicators were calculated, following community-accepted standards (IOCCG, 2006; Moore et al., 2009). These indicators included the coefficient of determination (R^2), mean absolute percentage error (ε), bias (δ), and root mean square error (RMSE) in log scale, defined as follows:

$$\varepsilon = \frac{1}{n}\sum_{i=1}^{n}\frac{|y_i - x_i|}{x_i} \times 100\,\% \qquad (1)$$

$$\delta = \frac{1}{n}\sum_{i=1}^{n}[\log_{10}(y_i) - \log_{10}(x_i)] \qquad (2)$$

BGD
10, 1–30, 2013

On the consistency in variations of chlorophyll *a* concentration

S. L. Shang et al.

Title Page
Abstract | Introduction
Conclusions | References
Tables | Figures
◂◂ | ▸▸
◂ | ▸
Back | Close
Full Screen / Esc
Printer-friendly Version
Interactive Discussion

cc BY

$$\text{RMSE} = \sqrt{\frac{1}{n}\sum_{i=1}^{n}[\log_{10}(y_i) - \log_{10}(x_i)]^2} \quad (3)$$

where x represents the measured parameter and y represents the algorithm-derived parameter.

3 Results

Figure 2 shows MODIS Chl distributions in three months during spring, summer, and winter. The images of fall are not shown because they are similar to those of spring. In general, all three Chl products showed consistent seasonality and spatial distributions: (1) Chl is lower in spring, higher in summer and winter; (2) Chl is lower in the offshore SCS (< 0.1–$\sim 0.1\,\text{mg}\,\text{m}^{-3}$) than in nearshore waters (~ 1–$> 1\,\text{mg}\,\text{m}^{-3}$); (3) there is a distinct band of elevated Chl off southwest Vietnam in summer, and a large patch of elevated Chl in and to the west of the Luzon Strait in winter. However, some apparent differences between the three products were also found, as shown in Figs. 2 and 3. The seasonality in C-GIOP was not as apparent as in C_OC3M or C_GSM. While C_OC3M and C_GSM showed maxima in winter, C-GIOP showed rather flat temporal changes between summer and winter. Field observations showed high Chl during winter (e.g. Chen, 2005; Ning et al., 2004), confirming the observed patterns in C_OC3M and C_GSM.

While Figs. 2 and 3 showed general patterns of the three Chl products, their consistency and discrepancy are detailed at several targeted locations, as shown below.

3.1 SEATS

The Southeast Asian Time-series Study station (SEATS, 18° N, 116° E), located in the deep (> 3000 m) oligotrophic basin, was used to represent the SCS offshore waters. All products showed similar seasonality of Chl, i.e., elevated Chl in winter (Fig. 4a).

This is consistent with in situ observations (Tseng et al., 2005). Very minor differences emerged in the detailed month-to-month and inter-annual variations (Fig. 4b). This is also illustrated by the strong correlation between C_GSM, C_GIOP and C_OC3M ($R > 0.8$). When compared with the limited in situ data (red dots in Fig. 4b), C_OC3M appeared to have the best performance (Fig. 4b). However, the difference mainly came from one data point in winter 2010 when both C_GSM and C_GIOP showed large departure from the in situ measurements. In general, all three Chl products showed consistent temporal patterns from this offshore SCS station.

3.2 Summer upwelling zones

The SCS is featured by upwelling in both summer and winter (e.g. Hong et al., 2009). The consistency of the three Chl products was examined in three well known summer upwelling zones, which are the upwelling zones off southwest Vietnam (VU), Qiongdong (QDU), and Yuedong (YDU) (See Fig. 1 for the locations).

The three Chl products showed the same upwelling features for the VU (Figs. 5 and 6). Propagation of the elevated Chl from June to August corresponded well to the propagation of the cool, upwelled water. This upwelling induced bloom was found to be specifically strong in August 2007, based on satellite Chl data from two sources (Liu et al., 2012). Our Fig. 6 told the same story.

Although the general patterns agreed with each other, the three products showed some differences in the mean monthly Chl extracted from the VU box (see Fig. 1, 10.5–14° N, 109–112° E) (Fig. 7). C_OC3M and C_GSM appeared to have stronger seasonality (i.e., larger difference between annual maximum and annual minimum) than C_GIOP. When the other two upwelling zones (QDU and YDU) were examined, similar phenomenon was also found (Fig. 8). In these two upwelling zones, winter highs were more distinct than summer highs based on C_OC3M and C_GSM, contradictory from the seasonal patterns observed from limited in situ measurements (e.g., Zhang et al., 1997).

CC BY

In short, all three Chl products revealed consistent Chl patterns associated with upwelling, but some discrepancies were found in their seasonality and inter-annual variations, especially between C_GIOP and the other two products. It is possible that Chl is overestimated in winter for C_OC3M and C_GSM, due to non-phytoplankton color matters commonly rich in this coastal water. This does not happen to the C_GIOP possibly because data alongshore are filtered during the process of producing the product.

3.3 Pearl River plume

There are two big rivers in the SCS, the Pearl River and the Mekong River. They contribute large amount of fresh water as well as nutrients and other matters to the nearby ocean, thus having significant impact on the biogeochemistry of the SCS. Here we chose the Pearl River plume as an example to examine the time-series derived from the three Chl data products.

Figure 9 (top) shows the monthly climatology of C_OC3M, C_GSM and C_GIOP in the vicinity of the Pearl River estuary (21–24° N, 112–118° E) in four months of different seasons. All three products consistently showed a distinct river plume extending eastward in summer.

To further compare the Chl products in nearshore waters, monthly climatology and monthly anomalies in January and July were extracted from waters shallower than 50 m. C_GIOP showed much lower monthly climatology than the other two products in both January and July because of the missing data of C_GIOP in some of the nearshore waters. For example, in January, C_GIOP was 0.26 $mg\,m^{-3}$ while C_OC3M was 2.20 $mg\,m^{-3}$. Furthermore, C_GSM was almost the same in January and July (3.42 versus 3.36 $mg\,m^{-3}$), a result contradictory to the known seasonal patterns.

The differences between the Chl products are further illustrated in the anomaly patterns (Fig. 9, bottom). In January, C_OC3M showed a strong positive anomaly in 2007, and C_GSM and C_GIOP appeared to have anomalies in the opposite directions. In July, the anomaly patterns of the three products were relatively similar to each other. A strong negative anomaly was found in 2004 in all three products, while the years of

CC BY

positive anomalies showed some discrepancy. Assuming that +25 % higher than climatology indicated a positive anomaly, a unique positive anomaly was found in 2009 for C_OC3M and C_GSM, while a > 25 % anomaly was found in 2008 for C_GIOP. Based on these observations, it could be inferred that summer blooms associated with river plumes and upwelling (e.g., Gan et al., 2010; Dai et al., 2008) were relatively weak in 2004. The bloom would however be inferred to be strong in 2009 if it was based on C_OC3M and C_GSM, or in 2008 if it was based on C_GIOP. Thus, without field-based validations (e.g., measured Chl, as river discharges, nutrient fluxes, wind forcing, etc.), interpretation of the satellite-based Chl data products requires extra caution for nearshore waters of the SCS.

Distributions of Chl anomaly patterns may be used to infer various nearshore and offshore physical processes. Figure 10 shows the spatial anomalies of the three Chl products. C_GIOP again appeared to be different from the other two. For example, the area of positive anomaly estimated from C_GIOP was $\sim 3.6 \times 10^4$ km^2 in July, while it ranged between 2.0×10^4–2.3×10^4 km^2 for the other two products. Stronger influence from river plumes and upwelling would thus then be inferred from C_GIOP than from the other two products. In January, C_OC3M showed the largest area with positive Chl anomaly ($\sim 2.8 \times 10^4$ km^2), while the other two products showed positive anomalies from $\sim 1.4 \times 10^4$ to $\sim 1.8 \times 10^4$ km^2. If the C_OC3M anomalies were compared between January and July (2.7×10^4 versus 2.3×10^4 km^2), one would infer that there were stronger coastal processes fostering phytoplankton growth in January than in July, which was unlikely true because 80 % of the Pearl River discharge takes place in the wet season (April–September) (PRWRC/PRRCC, 1991) and coastal upwelling also occurs in summer (Gan et al., 2010). Similarly, if the spatial anomaly patterns were used in empirical orthogonal function analysis to differentiate various physical processes (e.g. Yoder et al., 2002), different conclusion might result from the different Chl data products.

BGD
10, 1–30, 2013

CC BY

4 Discussion

The above results showed relatively consistent Chl patterns but higher difference in upwelling zones and river plumes from the three products. In order to diagnose the reasons of such similarity and discrepancy, in situ data were used to evaluate algorithm performance.

First, MODIS derived R_{rs} data were used as the algorithm inputs to derive Chl, and then compared with the measured Chl. Figure 11 shows the evaluation results where the statistics are listed in Table 1. The average percentage errors all exceeded the desired level of accuracy for satellite-derived Chl (35 %, Bailey and Werdell, 2006) in this dynamic marginal sea. Most of the MODIS derived Chl values were overestimated, as indicated by the large positive δ (>0.2). However, except for C_GIOP, MODIS derived Chl agreed with the in situ Chl reasonably well. The lower performance of C_GIOP is due in part to its poor performance in shallow waters (< 50 m, red dots in Fig. 11c).

To test whether the discrepancy resulted from the algorithms or from uncertainties in the MODIS R_{rs}, the accuracy of MODIS R_{rs} was evaluated using in situ R_{rs} (Fig. 12). In general, MODIS R_{rs} agreed well with ground truth data except at 412 nm and 667 nm. This is consistent from other reported results (e.g. Bailey and Werdell, 2006; Siegel et al., 2005; Antoine, 2008; Dong, 2010). R^2 ranged between 0.64–0.90 and ε was < 31 % for bands 443, 488, 531 and 547 nm, while R^2 was 0.44 for 412 nm and ε was 48.3 % for 667 nm. Because the 443, 488, and 547 nm bands were used to estimate Chl in the OC3M algorithm, the relatively lower uncertainties in the MODIS R_{rs} in these bands suggest that C_OC3M would be influenced less by the MODIS R_{rs} uncertainties than the other two products, which used the 412 and 667 bands to estimate Chl.

The uncertainties introduced by the algorithms were further examined by using in situ R_{rs} as the algorithm input, with the derived Chl compared with the measured Chl. Results are shown in Table 1 and Fig. 13. When compared with the field measured Chl, Chl derived from in situ R_{rs} agreed better than Chl derived from MODIS R_{rs} because of the reduction in the R_{rs} uncertainties and because of the removal of the mismatch

CC BY

between satellite pixel size and in situ sample size. Both OC3M and GSM performed well ($R^2 \sim 0.81$–0.85) although the error indices still exceeded the mission specifications (35 %). Similar to the above satellite-based analysis, GIOP showed lower R^2 and higher error indices than the other two algorithms (e.g., $\varepsilon \sim 256\,\%$). The results suggest that the uncertainties in the three Chl products were mostly attributed to the inversion algorithms as opposed to imperfect atmospheric correction. However, it is unclear what caused the relatively poor performance of the GIOP algorithm in this marginal sea. Indeed, in an algorithm round-robin comparison, all 17 algorithms including GIOP were found to perform reasonably well in estimating Chl (Brewin et al., 2013). We speculate that the algorithm parameterization of GIOP requires a major tuning for the study region.

Thus, differences in the MODIS Chl data products appeared to have resulted mainly from the algorithm design in addressing the dependence of reflectance on the various in-water constituents. In the offshore SCS, optical properties are predominantly driven by phytoplankton, and the three Chl products showed almost the same spatial and temporal patterns although their magnitudes varied slightly. In coastal upwelling zones and river plumes where the water is optically complex with significant amount of colored dissolved organic matter (CDOM) and inorganic particles (Hong et al., 2005; Du et al., 2010), larger differences were found from the three Chl products. The OC3M empirical algorithm was not designed to differentiate Chl from other in-water constituents. The spectral optimization algorithms such as GSM and GIOP were designed to separate Chl from other in-water constituents, yet their performance was influenced by their fixed parameterization (IOCCG, 2006). Failure in finding an optimal solution may be one reason to cause pixel speckling in the C_GSM images and those masked nearshore pixels in the C_GIOP images (Fig. 9 top). These failed pixels would cause a bias in calculating the mean and anomalies. Clearly, when time-series data were analyzed, image series would need to be examined in order to identify these potential artifacts and to improve data interpretation.

BGD
10, 1–30, 2013

CC BY

5 Conclusions

Three MODIS Chl products are currently being used by the research community to address global and regional questions. These are derived from the OC3M, GSM, and GIOP algorithms. Yet their accuracy and consistency between each other are often unclear for marginal seas. Using a large field dataset collected from the SCS, we evaluate the accuracy of the three MODIS Chl data products as well as their consistency in revealing spatial and temporal patterns under various scenarios.

The in situ validation showed RMS errors > 0.3 in log scale and percentage errors $> 80\,\%$ for all three Chl products, while nearly identical statistical results were found for OC3M and GSM. GIOP showed significant deviation from the ground truth, possibly due to the incompatibility between its default parameterization and the optical properties of the SCS.

The temporal changes and spatial distribution patterns in the three Chl data products differ mainly in optically complex nearshore waters because the algorithms were designed to address optical complexity differently. Such a difference is attributed to mainly the algorithm design as opposed to the uncertainties in the input R_{rs}. In offshore SCS waters where optical properties are dominated by phytoplankton, Chl seasonality and inter-annual changes derived from the three products were similar. The findings here suggest that continuous improvements in remote sensing algorithms are still required in order to minimize the discrepancies in the various Chl data products and to reduce uncertainties of these products.

Acknowledgements. This work was supported jointly by NSF-China (#40976068) and the National Basic Research Program of China (#2009CB421201). We thank the crew of the R/V Dongfanghong II and Yanping II, and Jingyu Wu, Xiaoxin Ma, Xiaofei Sui, Wen Zhou, Wenqi Wang, Min Yang, Cuifen Du and Guomei Wei for their help in collecting in situ data. We also thank the NASA OBPG for providing MODIS data.

CC BY

References

Antoine, D.: Assessment of uncertainty in the ocean reflectance determined by three satellite ocean color sensors (MERIS, SeaWiFS and MODIS-A) at an offshore site in the Mediterranean Sea (BOUSSOLE project), J. Geophys. Res., 113, C07013, doi:10.1029/2007JC004472, 2008.

Bailey, S. W. and Werdell, P. J.: A multi-sensor approach for the on-orbit validation of ocean color satellite data products, Remote Sens. Environ., 102, 12–23, 2006.

Behrenfeld, M. J. and Boss, E.: Beam attenuation and chlorophyll concentration as alternative optical indices of phytoplankton biomass, J. Mar. Res., 64, 431–451, 2006.

Brewin, R. J., Dall'Olmo, G., Sathyendranath, S., and Hardman-Mountford, N. J.: Particle backscattering as a function of chlorophyll and phytoplankton size structure in the open-ocean, Opt. Express, 20, 17632–17652, 2012.

Brewin, R. J., Sathyendranath, S., Müller, D., Brockmann, C., Deschampse, P., Devred, E., Doerffer, R., Fomferra, N., Franz, B., Grant, M., Groom, S., Horseman, A., Hu, C., Krasemann, H., Lee, Z., Maritorena, S., Mélink, F., Peters, M., Platt, T., Regner, P., Smyth, T., Steinmetz, F., Swinton, J., Werdell, J., and White, G.: The ocean colour climate change initiative: a round-robin comparison on in-water bio-optical algorithms, submitted, 2013.

Carder, K. L., Steward, R. G., Harvey, G. R., and Ortner, P. B.: Marine humic and fulvic acids: their effects on remote sensing of ocean chlorophyll, Limnol. Oceanogr., 34, 68–81, 1989.

Chen, L.: Spatial and seasonal variations of nitrate-based new production and primary production in the South China Sea, Deep Sea Res. Pt. I, 52, 319–340, 2005.

Cullen, J. J.: The deep chlorophyll maximum: comparing vertical profiles of chlorophyll *a*, Can. J. Fish. Aquat. Sci., 39, 791–803, 1982.

Dai, M. H., Zhai, W. D., Cai, W. J., Callahan, J., Huang, B. Q., Shang, S. L., Huang, T., Li, X. L., Lu, Z. M., Chen, W. F., and Chen, Z. Z.: Effects of an estuarine plume-associated bloom on the carbonate system in the lower reaches of the Pearl River estuary and the coastal zone of the northern South China Sea, Cont. Shelf Res., 28, 1416–1423, doi:10.1016/j.csr.2007.04.018, 2008.

Dong, Q.: Derivation of Phytoplankton Absorption Properties from Ocean Color and Its Application, Ph.D. thesis, Xiamen University, Xiamen, China, 2010.

BGD

10, 1–30, 2013

CC BY

Du, C. F., Shang, S. L., Dong, Q., Hu, C. M., and Wu, J. Y.: Characteristics of chromophoric dissolved organic matter in the nearshore waters of the western Taiwan Strait, Estuar. Coast. Shelf S., 88, 350–356, doi:10.1016/j.ecss.2010.04.014, 2010.

Franz, B. A. and Werdell, P. J.: A generalized framework for modeling of inherent optical properties in ocean remote sensing applications, Ocean Optics XX, Anchorage, Alaska, 27 Sep–1 Oct, 2010.

Gan, J. P., Lu, Z. M., Dai, M. H., Cheung, A. Y. Y., Liu, H. B., and Harrison, P.: Biological response to intensified upwelling and to a river plume in the northeastern South China Sea: A modeling study, J. Geophys. Res.-Oceans, 115, C09001, doi:10.1029/2009jc005569, 2010.

Hirawake, T., Takao, S., Horimoto, N., Ishimaru, T., Yamaguchi, Y., and Fukuchi, M.: A phytoplankton absorption-based primary productivity model for remote sensing in the Southern Ocean, Polar Biol., 34, 291–302, 2011.

Hong, H., Wu, J., Shang, S., and Hu, C.: Absorption and fluorescence of chromophoric dissolved organic matter in the Pearl River Estuary, South China, Mar. Chem., 97, 78–89, 2005.

Hong, H., Zhang, C., Shang, S., Huang, B., Li, Y., Li, X., and Zhang, S.: Interannual variability of summer coastal upwelling in the Taiwan Strait, Cont. Shelf Res., 29, 479–484, 2009.

Hong, H., Liu, X., Chiang, K.-P., Huang, B., Zhang, C., Hu, J., and Li, Y.: The coupling of temporal and spatial variations of chlorophyll a concentration and the East Asian monsoons in the southern Taiwan Strait, Cont. Shelf Res., 31, S37–S47, doi:10.1016/j.csr.2011.02.004, 2011.

IOCCG: Remote sensing of inherent optical properties: fundamentals, tests of algorithms, and applications, in: Reports of the International Ocean-Colour Coordinating Group, No. 5, edited by: Lee, Z. P., IOCCG, Dartmouth, Canada, 126 pp., 2006.

Lalli, C. M. and Parsons, T. R.: Biological Oceanography: An Introduction, Pergamon Press, Oxford, 1993.

Lee, Z. P., Du, K., Voss, K. J., Zibordi, G., Lubac, B., Arnone, R., and Weidemann, A.: An IOP-centered approach to correct the angular effects in water-leaving radiance, Appl. Optics., 50, 3155–3167, 2011.

Lin, I. I., Lien, C. C., Wu, C. R., Wong, G. T., Huang, C. W., and Chiang, T. L.: Enhanced primary production in the oligotrophic South China Sea by eddy injection in spring, Geophys. Res. Lett., 37, L16602, doi:10.1029/2010GL043872, 2010.

CC BY

Liu, X., Wang, J., Cheng, X., and Du, Y.: Abnormal upwelling and chlorophyll *a* concentration off South Vietnam in summer 2007, J. Geophys. Res.-Oceans, 117, C07021, 10.1029/2012JC008052, 2012.

Maritorena, S., Siegel, D. A., and Peterson, A. R.: Optimization of a semianalytical ocean color model for global-scale applications, Appl. Optics, 41, 2705–2714, 2002.

Marra, J., Trees, C. C., and O'Reilly, J. E.: Phytoplankton pigment absorption: a strong predictor of primary productivity in the surface ocean, Deep-Sea Res. Pt. I, 54, 155–163, 2007.

McClain, C. R.: A decade of satellite ocean color observations*, Annu. Rev. Mar. Sci., 1, 19–42, 2009.

Moore, T. S., Campbell, J. W., and Dowell, M. D.: A class-based approach to characterizing and mapping the uncertainty of the MODIS ocean chlorophyll product, Remote Sens. Environ., 113, 2424–2430, 2009.

Ning, X., Chai, F., Xue, H., Cai, Y., Liu, C., and Shi, J.: Physical-biological oceanographic coupling influencing phytoplankton and primary production in the South China Sea, J. Geophys. Res., 109, C10005, doi:10.1029/2004JC002365, 2004.

O'Reilly, J., Maritorena, S., Mitchell, B. G., Siegel, D., Carder, K. L., Garver, S., Kahru, M., and McClain, C.: Ocean color chlorophyll algorithms for SeaWiFS, J. Geophys. Res., 103, 24937–24953, 1998.

O'Reilly, J. E., Maritorena, S., Siegel, D., and O'Brien, M. C.: Ocean color chlorophyll a algorithms for SeaWiFS, OC2, and OC4: version 4, in: SeaWiFS postlaunch technical report series, volume 11, SeaWiFS postlaunch calibration and validation analyses, part 3, edited by: Hooker, S. B. and Firestone, E. R., Greenbelt, Maryland: NASA Goddard Space Flight Center, 9–23, 2000.

Palacz, A. P., Xue, H., Armbrecht, C., Zhang, C., and Chai, F.: Seasonal and inter-annual changes in the surface chlorophyll of the South China Sea, J. Geophys. Res.-Oceans, 116, C09015, 10.1029/2011JC007064, 2011.

PRWRC/PRRCC: The Pearl River Records (Zhujiang Zhi), Guangzhou, China, 357 pp., 1991.

Shang, S., Dong, Q., Lee, Z., Li, Y., Xie, Y., and Behrenfeld, M.: MODIS observed phytoplankton dynamics in the Taiwan Strait: an absorption-based analysis, Biogeosciences, 8, 841–850, doi:10.5194/bg-8-841-2011, 2011.

Siegel, D. A., Maritorena, S., Nelson, N. B., and Behrenfeld, M. J.: Independence and interdependencies among global ocean color properties: Reassessing the bio-optical assumption, J. Geophys. Res., 110, C07011, doi:10.1029/2004JC002527, 2005.

Tseng, C. M., Wong, G. T. F., Lin, I. I., Wu, C. R., and Liu, K. K.: A unique seasonal pattern in phytoplankton biomass in low-latitude waters in the South China Sea, Geophys. Res. Lett., 32, L08608, doi:10.1029/2004GL022111, 2005.
Werdell, P. J.: Global bio-optical algorithms for ocean color satellite applications, EOS T. Am. Geophys. Un., 90, doi:10.1029/2009EO010005, 2009.
Xiu, P. and Chai, F.: Modeled biogeochemical responses to mesoscale eddies in the South China Sea, J. Geophys. Res.-Oceans, 116, C10006, 10.1029/2010JC006800, 2011.
Yoder, J. A., Schollaert, S. E., and O'Reilly, J. E.: Climatological phytoplankton chlorophyll and sea surface temperature patterns in continental shelf and slope waters off the northeast US coast, Limnol. Oceanogr., 47, 672–682, 2002.
Zhang, F., Y. Yang and B. Q. Huang.: Impact of nutrients on the chlorophyll *a* concentration in the Taiwan Strait. In: Collection of Oceanography Research (7), edited by: Hong, H. S., Beijing, Ocean Press., 81–88, 1997 (in Chinese with English abstract).

BGD
10, 1–30, 2013

Title Page
Abstract | Introduction
Conclusions | References
Tables | Figures
◀| |▶
◀ ▶
Back | Close
Full Screen / Esc
Printer-friendly Version
Interactive Discussion

CC BY

Table 1. Error statistics between derived and in situ Chl concentration.

Algorithm	R^2	ε(%)	RMSE	δ	N	n
MODIS R_{rs} derived (in situ Chl = 0.03–7.67 mg m^{-3}, mean = 2.89, std= 1.32)						
OC3M	0.53	158	0.410	0.249	63	63
GSM	0.53	145	0.402	0.208	63	63
GIOP	0.50	349	0.616	0.449	63	62
MODIS R_{rs} derived (< 50 m) (Chl = 0.11–7.67 mg m^{-3}, mean = 0.85, std = 1.60)						
OC3M	0.46	224	0.496	0.342	36	36
GSM	0.46	210	0.491	0.312	36	36
GIOP	0.42	519	0.754	0.617	36	35
In situ R_{rs} derived (Chl = 0.03–51.15 mg m^{-3}, mean = 1.25, std= 6.63)						
OC3M	0.81	111	0.363	0.132	192	192
GSM	0.85	94	0.342	0.086	192	174
GIOP	0.13	256	0.548	0.163	192	160

N is the number of R_{rs} data input, while n is the number of valid retrievals.

Discussion Paper | Discussion Paper | Discussion Paper | Discussion Paper |

BGD

10, 1–30, 2013

On the consistency in variations of chlorophyll *a* concentration

S. L. Shang et al.

Title Page
Abstract Introduction
Conclusions References
Tables Figures
◀◀ ▶▶
◀ ▶
Back Close
Full Screen / Esc

Printer-friendly Version

Interactive Discussion

CC BY

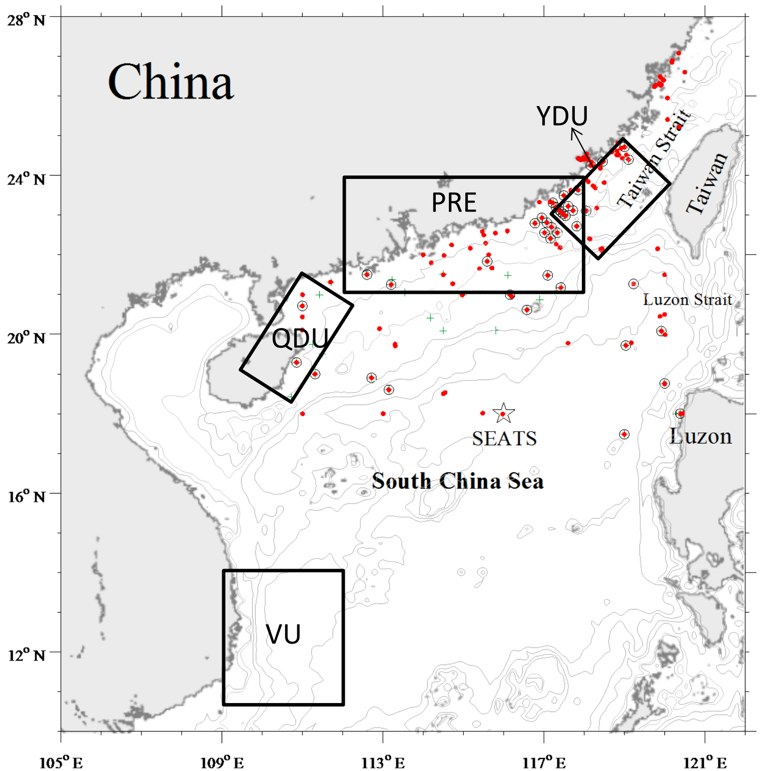

Fig. 1. Map of the study region. VU, QDU and YDU refer to upwelling zones off Vietnam, Qiongdong, and Yuedong (boundaries of the zones were defined following Jing et al., 2011). PRE refers to the Pearl River Estuary, and SEATS refers to the Southeast Asian Time-series Study station (18° N, 116° E). Black empty circles show the locations where concurrent MODIS and in situ R_{rs} data were extracted for comparison. Green crosses show the locations where concurrent MODIS R_{rs} data and in situ observed Chl were used for algorithm evaluations. Red circles show the locations where field measured R_{rs} and Chl were used for algorithm evaluations.

BGD
10, 1–30, 2013

CC BY

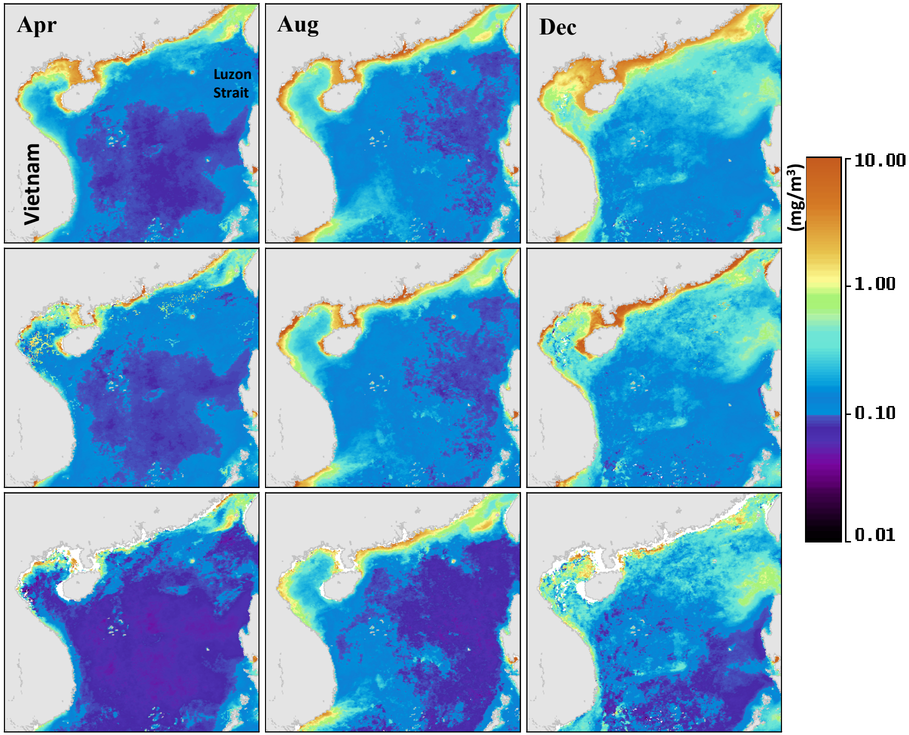

Fig. 2. Climatological monthly mean Chl in the South China Sea in April, August and December from three algorithms: (top) C_OC3M; (middle) C_GSM; (bottom) C_GIOP.

BGD
10, 1–30, 2013

CC BY

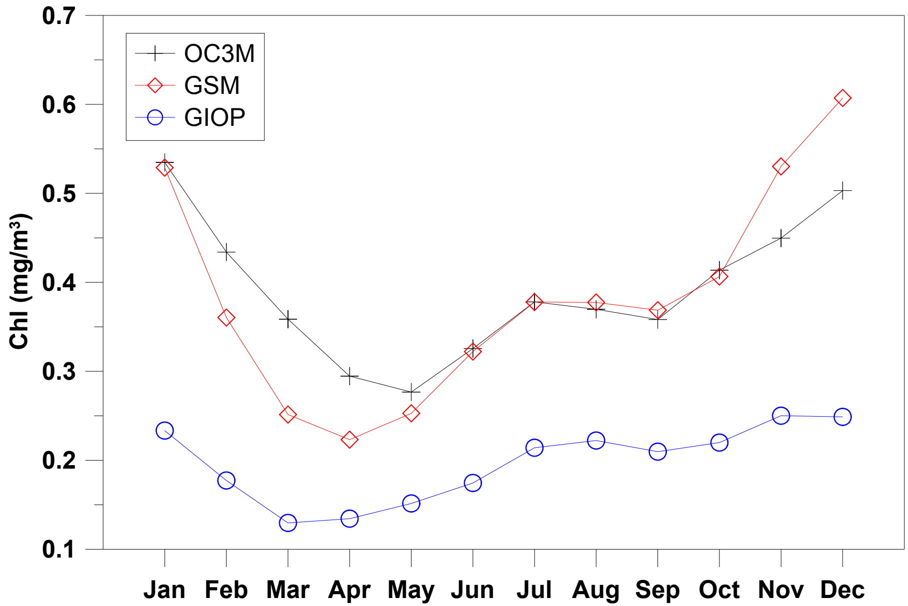

Fig. 3. Monthly climatology of MODIS Chl for the South China Sea.

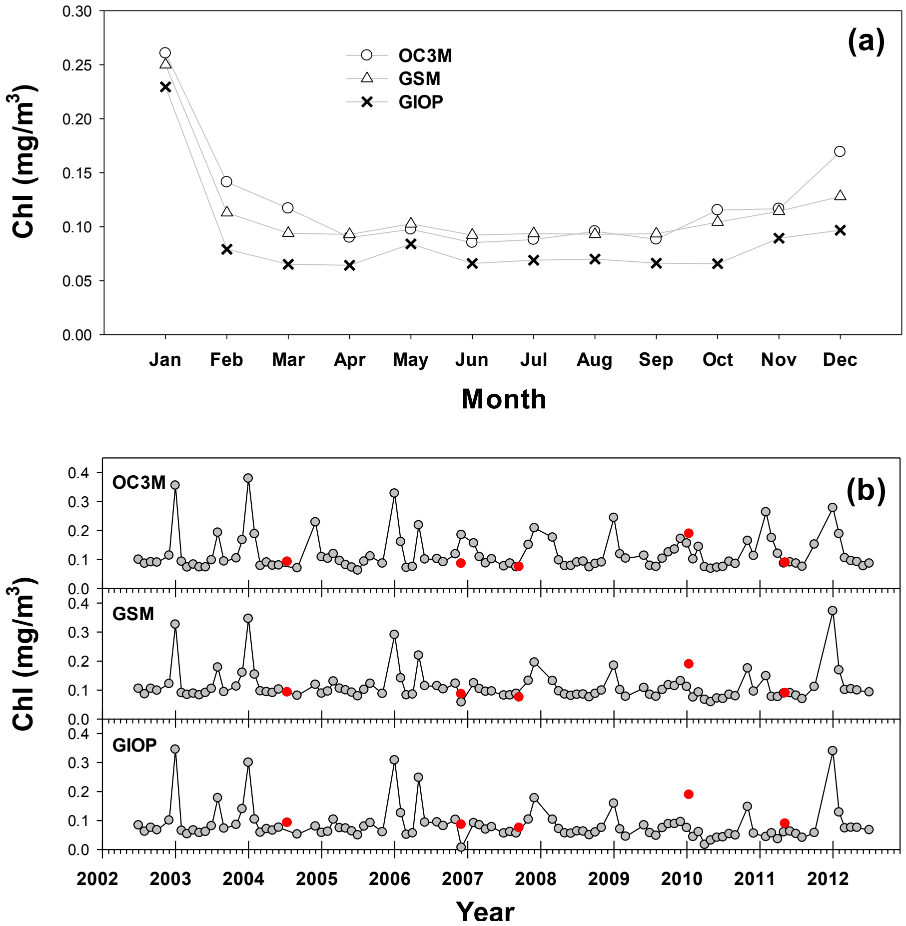

Fig. 4. Monthly climatology **(a)** and monthly variations **(b)** of MODIS Chl at SEATS. Red symbols refer to field measured Chl.

BGD
10, 1–30, 2013

CC BY

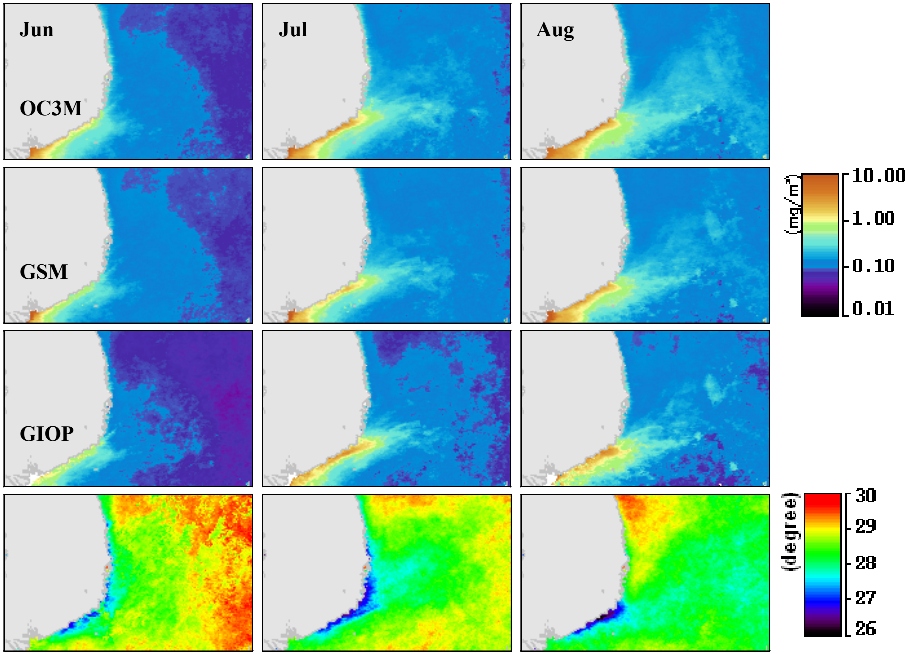

Fig. 5. Climatological monthly mean Chl and SST derived from MODIS measurements in June–August for the region of 10–15° N, 106–114° E.

BGD
10, 1–30, 2013

On the consistency in variations of chlorophyll *a* concentration

S. L. Shang et al.

cc BY

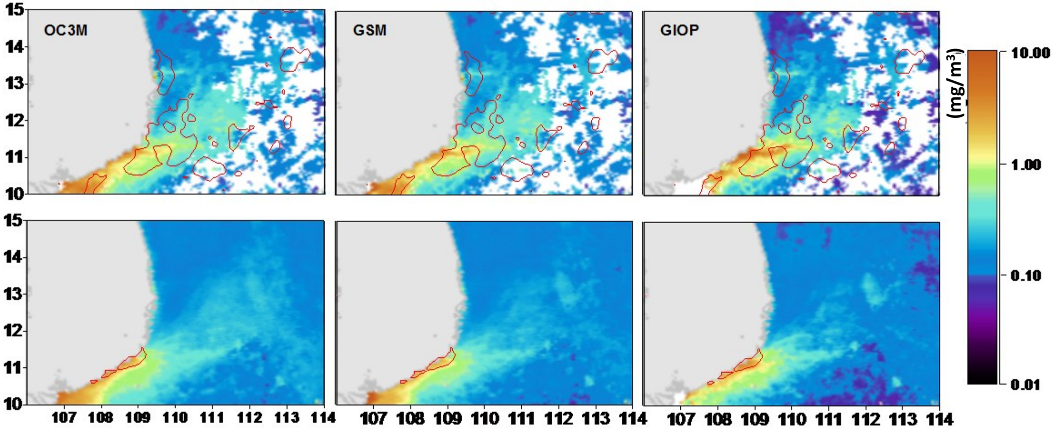

Fig. 6. MODIS Chl imagery showing elevated Chl in coastal waters off southwest Vietnam: August 2007 (top row) compared with the August Chl climatology (bottom row). Overlaid contours are the MODIS SST of 27 °C.

BGD
10, 1–30, 2013

On the consistency in variations of chlorophyll *a* concentration

S. L. Shang et al.

Title Page
Abstract Introduction
Conclusions References
Tables Figures
◀▌ ▶▌
◀ ▶
Back Close
Full Screen / Esc
Printer-friendly Version
Interactive Discussion

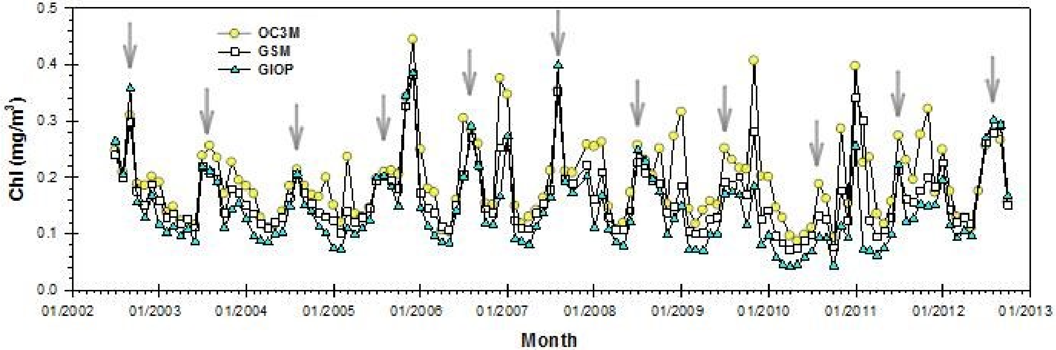

Fig. 7. Monthly variations of MODIS Chl in the upwelling zone off southwest Vietnam; arrows indicate summer.

CC BY

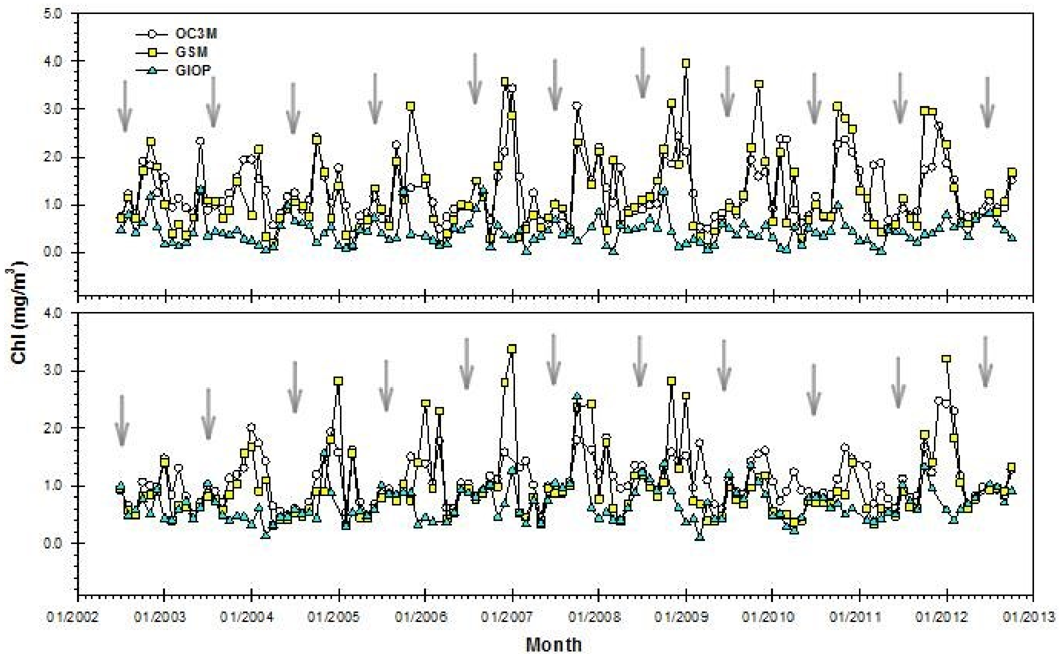

Fig. 8. Monthly variations of MODIS Chl in the QD **(a)** and YD **(b)** upwelling zones; arrows indicate summer.

CC BY

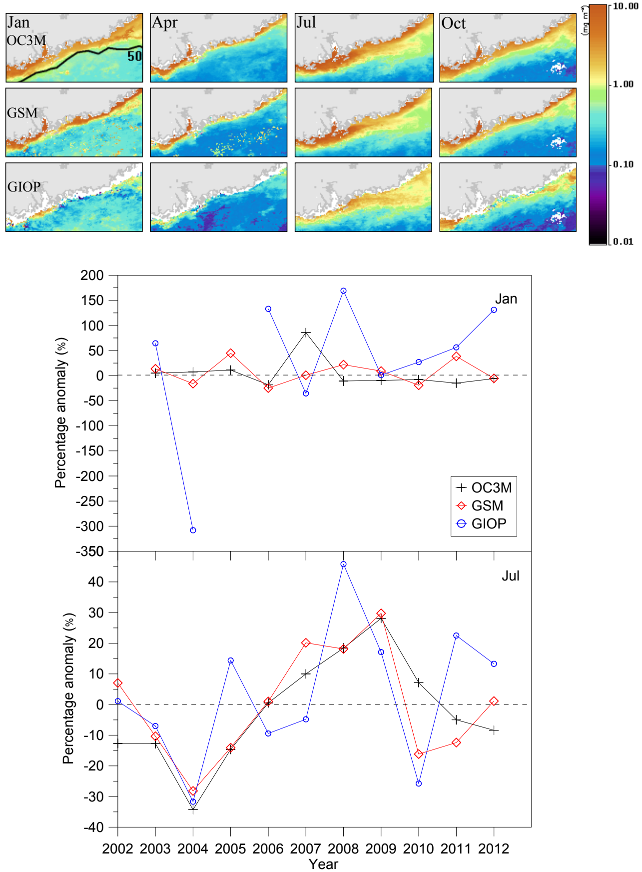

Fig. 9. (Top) Monthly climatology of MODIS Chl in the vicinity of the Pearl River estuary in January, April, July and October. The isobath of 50 m was annotated on the January image of C_OC3M; (Bottom) MODIS Chl anomaly (in percentage) in January and July of 2002–2012 for the nearshore waters of the PRE (depth < 50 m).

BGD
10, 1–30, 2013

CC BY

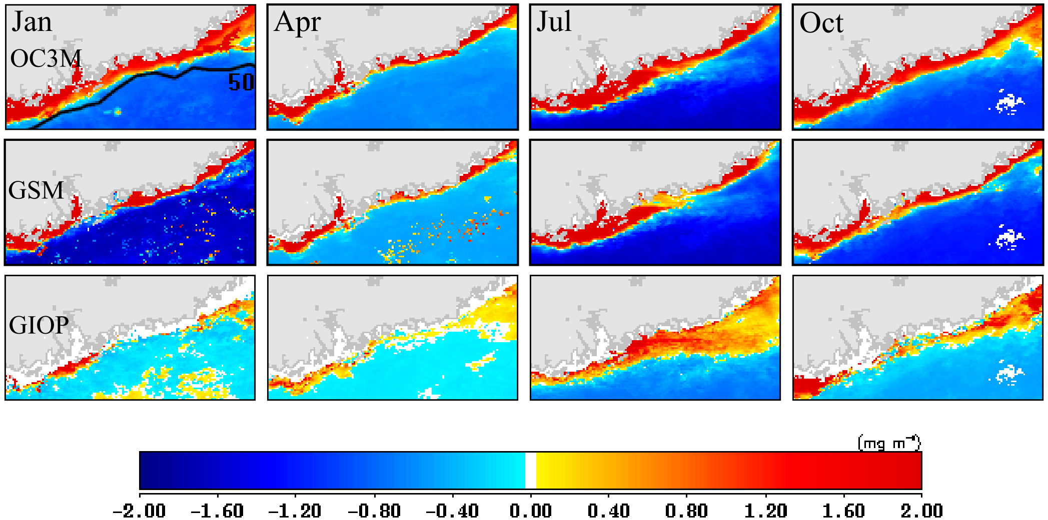

Fig. 10. MODIS Chl anomaly in the vicinity of the PRE in January, April, July and October. The isobath of 50 m was annotated on the January image of C_OC3M.

CC BY

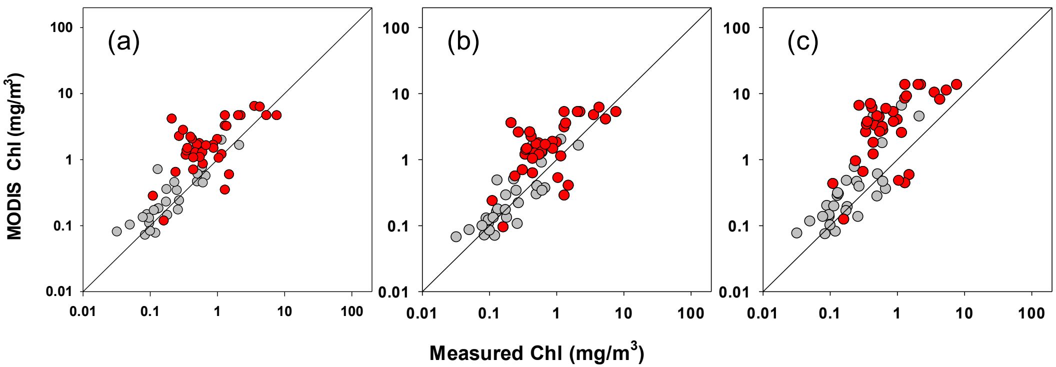

Fig. 11. Comparison between MODIS R_{rs} derived Chl and field measured Chl where MODIS Chl was derived using three algorithms: **(a)** OC3M; **(b)** GSM; **(c)** GIOP. Red symbols refer to data collected from nearshore waters (depth < 50 m). Statistics of the algorithm performance are listed in Table 1.

CC BY

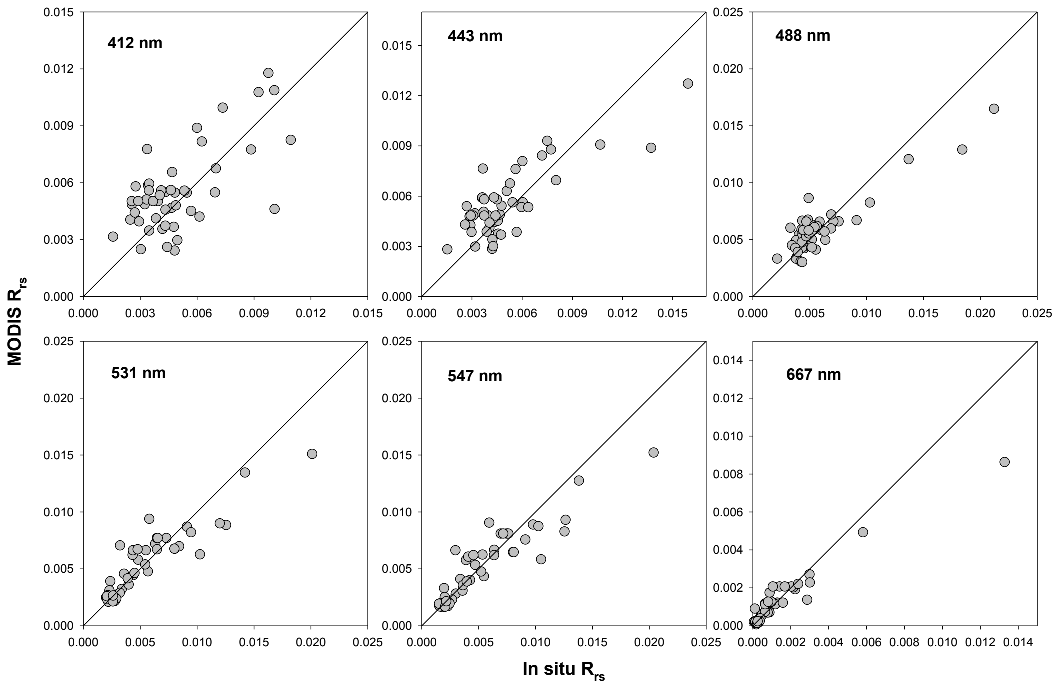

Fig. 12. Comparison between MODIS-derived R_{rs} and field measured R_{rs}.

BGD
10, 1–30, 2013

On the consistency in variations of chlorophyll *a* concentration

S. L. Shang et al.

CC BY

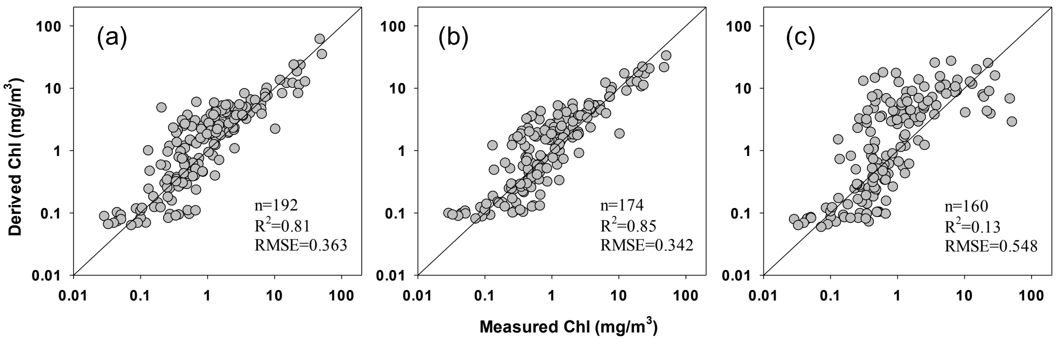

Fig. 13. Comparison between field measured Chl and in situ R_{rs} derived Chl using three algorithms: **(a)** OC3M; **(b)** GSM; **(c)** GIOP. Statistics of algorithm performance are listed in Table 1.

CC BY